On the Aerodynamic Heating of a KE Penetrator—Conductive Material Heating and Thermal Gradients Prior to Transient Impact Loading

by Todd W. Bjerke

20011005 107

Army Research Laboratory

Aberdeen Proving Ground, MD 21005-5066

On the Aerodynamic Heating of a KE Penetrator — Conductive Material Heating and Thermal Gradients Prior to Transient Impact Loading

Todd W. Bjerke
Weapons and Materials Research Directorate, ARL

Abstract

The temperature increase in the main body portion of a kinetic energy penetrator flying at sea level with a speed of 1,500 m/s was calculated using an analytical conduction analysis with a convective boundary condition. The penetrator was modeled as a smooth cylinder of uniform diameter and material properties. The results from a previously published computational fluid dynamics simulation were used to provide the convective heat transfer coefficient and the temperature of the gas flowing over the surface of the penetrator. A separation of variables solution was used for the parabolic time-dependent conduction equation. The derived solution along with material properties for tungsten and depleted uranium were used to obtain the temperature increase profile through the radius of the penetrator as a function of flight time. Both materials showed significant heating within 3 s of flight. The tungsten penetrator exhibited nearly uniform heating across the radius, whereas heating of the depleted uranium penetrator was confined to the outermost region of the cylinder due to its low coefficient of thermal conductivity.

Contents

INTENTIONALLY LEFT BLANK.

List of Figures

INTENTIONALLY LEFT BLANK.

List of Tables

INTENTIONALLY LEFT BLANK.

1. Introduction

A kinetic energy (KE) penetrator launched from a cannon travels to its intended target typically at speeds in excess of 1,500 m/s. At these velocities, the adiabatic wall temperature of the air reaches approximately 1300 K (Guidos and Weinacht 1993), establishing the potential for increasing the temperature of the penetrator. If the temperature of the penetrator is significantly increased, the mechanical behavior of the penetrator material will change, thereby affecting terminal ballistic performance (Magness and Lopatin 1993). Two metallic alloys commonly used for KE penetrators are tungsten heavy alloys (WHA) that generally contain greater than 90% (by weight) tungsten and depleted uranium (DU) alloyed with less than 1% titanium. The yield stress of these materials has been observed to decrease exponentially with temperature (Zurek and Follansbee 1995). Fracture properties and fracture mode are temperature sensitive as well. In particular, the ductile-brittle transition temperature for WHA is at room temperature or slightly above, depending upon composition, stress state, and strain rate (Larson and DeLai 1980; Gurwell 1986). The ductile-brittle transition temperature of unalloyed uranium is 0 °C (Eckelmeyer 1991), with the transition temperature of DU expected to be slightly lower. An important consequence of this transition temperature is that the mode of fracture during target interaction will change depending on the penetrator flight distance. More significantly, the terminal ballistic efficacy of a KE penetrator may depend on the penetrator-target engagement distance. For these reasons, it is necessary to know the penetrator temperature history during flight.

The flow field over a KE penetrator moving at supersonic and hypersonic speeds was determined by Guidos and Weinacht (1993) using a three-dimensional, parbolized Navier-Stokes computational technique. Their numerical simulations provided perfect gas heat transfer parameters for a penetrator of geometry similar to the M829. Penetrator speed was 1,500 m/s. The adiabatic wall temperatures and the convective heat transfer coefficients reported by Guidos and Weinacht provide the boundary conditions needed for transient conduction analyses to quantify the penetrator temperature history. The results contained within this report were obtained by solving a one-dimensional transient heat conduction equation that uses the Guidos and Weinacht boundary conditions. Only the cylindrical main body portion of the penetrator was considered for the conduction solution.

2. Conduction Model and Solution Technique

2.1 One-Dimensional Conduction Model

The heat transfer model used to describe the temperature increase of a KE penetrator traveling through shock-heated air consists of a governing equation derived from the first law of thermodynamics and Fourier's law, and a set of initial and boundary conditions. The general conduction model and its solution can be found in advanced heat conduction texts (see Poulikakos [1994] for example). It is derived here for completeness and to fully document the assumptions and modeling simplifications that were made and the solution technique used. The heat conduction equation obtained from the rate form of energy conservation is given as

$$\frac{\partial T}{\partial t} = \alpha \nabla^2 T + \dot{Q}_{gen},\tag{1}$$

where T is temperature, t is time, $\dot{Q}_{gen}$ is the rate of internal heat generation per unit volume, and α is the thermal diffusivity defined as $\alpha = k/\rho c$ (k is the thermal conductivity, ρ is the bulk density, and c is the specific heat). Note that compressibility effects are neglected in equation 1, implying ρ = constant and $c_p = c_v = c$ (where c_p and c_v are the specific heat at constant pressure and volume, respectively), and that the thermal conductivity of the material is assumed constant. As will be seen, it shall be convenient to work in a cylindrical coordinate system (r, θ, z). In cylindrical coordinates, equation (2) has the following form:

$$\frac{\partial T}{\partial t} = \alpha\left[\frac{1}{r}\frac{\partial T}{\partial r} + \frac{\partial^2 T}{\partial r^2} + \frac{1}{r^2}\frac{\partial^2 T}{\partial \theta^2} + \frac{\partial^2 T}{\partial z^2}\right] + \dot{Q}_{gen}.\tag{2}$$

Equation 2 can be simplified by considering the geometry of a typical KE penetrator, shown in Figure 1. The penetrator main body was simplified to a right-circular cylinder of length L and radius R, with a smooth surface (as was also done in the computational model of Guidos and Weinacht [1993]). Since the focus of this effort is to identify the temperature history of the main body, effects from the nose cap and fin were neglected. This leads to the penetrator configuration and heating process depicted in Figure 2, which is amenable to description in a cylindrical coordinate system. Noting symmetry in the θ plane, the transient heat conduction is at most two-dimensional, occurring in the r-z plane. Scaling arguments show that

$$\frac{\partial^2 T}{\partial r^2} \sim O\left(\frac{T_0 - T_\infty}{R^2}\right)\tag{3}$$

and
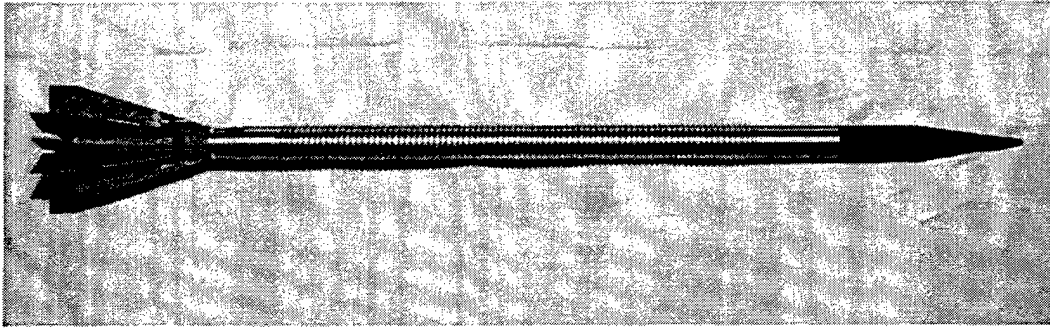
Figure 1. Geometry of a typical KE penetrator.
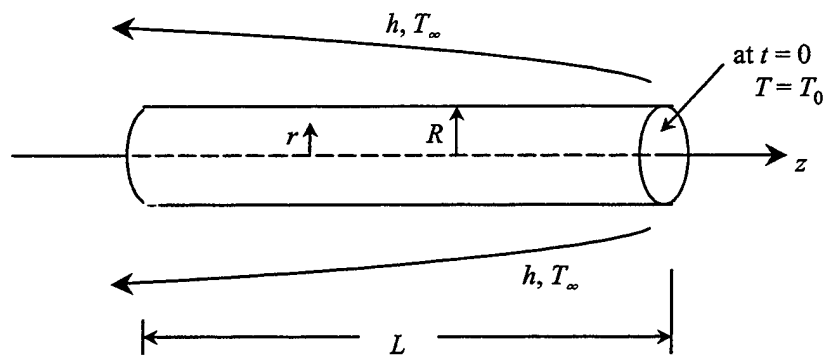
Figure 2. Simplified penetrator for heat transfer model.

$$\frac{\partial^2 T}{\partial z^2} \sim O\left(\frac{T_0 - T_\infty}{L^2}\right). \tag{4}$$

Since $L >> R$, equations 3 and 4 imply that

$$\frac{\partial^2 T}{\partial r^2} >> \frac{\partial^2 T}{\partial z^2}. \tag{5}$$

Therefore, the heat conduction equation expressed in cylindrical coordinates (2) reduces to the following one-dimensional governing equation (neglecting internal heat generation):

$$\frac{1}{\alpha}\frac{\partial T}{\partial t} = \frac{1}{r}\frac{\partial T}{\partial r} + \frac{\partial^2 T}{\partial r^2}. \tag{6}$$

One initial condition and two boundary conditions are required for solving equation 6. The initial condition is a statement that the penetrator is at ambient temperature when $t = 0$. The first boundary condition is recognizing that there is no

heat flux at the centerline of the penetrator, i.e., a symmetry condition. The final boundary condition is obtained by noting that if a body is in contact with a moving convective fluid, the heat conduction in the body equals the heat convected by the fluid. Mathematically, the initial and boundary statements are the following:

$$t = 0 : T = T_0,$$ (7)

$$r = 0 : \frac{\partial T}{\partial r} = 0,$$ (8)

and

$$r = R : -k\frac{\partial T}{\partial r} = h(T - T_\infty),$$ (9)

where T_0 is the initial temperature of the penetrator, T_∞ is the temperature of the shock heated air, and h is the convective heat transfer coefficient. The method of separation of variables will be used to solve the one dimensional conduction equation 6. For this method to apply, the governing equation as well as both boundary conditions must be homogeneous. While equations 6 and 8 are homogeneous, equation 9 is not. To remedy this situation, the following variable substitution is used:

$$\Theta = T - T_\infty.$$ (10)

Expressing the governing equation, boundary, and initial conditions in terms of this new variable yields

$$\frac{1}{\alpha}\frac{\partial \Theta}{\partial t} = \frac{1}{r}\frac{\partial \Theta}{\partial r} + \frac{\partial^2 \Theta}{\partial r^2},$$ (11)

$$t = 0 : \Theta = T_0 - T_\infty = \Theta_0,$$ (12)

$$r = 0 : \frac{\partial \Theta}{\partial r} = 0,$$ (13)

and

$$r = R : -k\frac{\partial \Theta}{\partial r} = h\Theta.$$ (14)

Proceeding with the separation of variables solution, let Θ be of the product form

$$\Theta(r,t) = F(r)G(t),$$ (15)

where the functions $F(r)$ and $G(t)$ are to be determined. Putting the assumed form of Θ from equation 15 into the governing equation 11 and performing the standard separation of variables analysis (see Greenberg [1988] for additional details) yields the following two ordinary differential equations

4

$$F'' + \frac{1}{r}F' + \lambda^2 F = 0 \tag{16}$$

and

$$G' + \alpha\lambda^2 G = 0, \tag{17}$$

where the eigenvalue λ remains to be determined. The solutions to equations 16 and 17 are

$$F = A J_0(\lambda r) + B Y_0(\lambda r) \tag{18}$$

and

$$G = C e^{-\lambda^2 \alpha t}, \tag{19}$$

where J_0 is the Bessel function of the first kind of order zero, Y_0 is the Bessel function of the second kind of order zero, and A, B, and C are unknown constants. Substituting equations 18 and 19 into equation 15 and combining constants gives the general solution

$$\Theta = [E J_0(\lambda r) + D Y_0(\lambda r)] e^{-\lambda^2 \alpha t}, \tag{20}$$

where $E = AC$ and $D = BC$. Applying of the boundary condition at $r = 0$, given by equation 13, yields

$$D = 0. \tag{21}$$

The value of λ is determined by substituting equation 20 into the convective boundary condition (equation 14), which gives the following expression

$$(\lambda_n R) J_1(\lambda_n R) = Bi\, J_0(\lambda_n R) \qquad n = 1,2,3,...., \tag{22}$$

where the subscript n denotes the fact that an infinite number of eigenvalues λ_n satisfy equation 22, J_1 is the Bessel function of the first kind of first order, and the Biot number is defined as

$$Bi = \frac{hR}{k}. \tag{23}$$

Since R and the Biot number are known values, the eigenvalues can be obtained by solving equation 22 numerically or graphically. A graphical technique was used and is discussed in section 2.2. With the eigenvalues known, the general solution becomes

$$\Theta = \sum_{n=1}^{\infty} E_n J_0(\lambda_n r) e^{-\lambda_n^2 \alpha t}. \tag{24}$$

An expression for the last unknown constant, E_n, is obtained by using the initial condition (equation 12). Substituting equation 24 into equation 12 gives

$$\Theta_0 = \sum_{n=1}^{\infty} E_n J_0(\lambda_n r). \tag{25}$$

An explicit expression for E_n can be obtained by multiplying both sides of equation 25 by $rJ_0(\lambda_n r)$, integrating both sides from $r = 0$ to $r = R$, and using the fact that the family of Bessel functions $J_0(\lambda_n r)$ are orthogonal with respect to the weighting factor r (see Poulikakos [1994] for details). The resulting expression is

$$E_n = \frac{2\Theta_0}{J_0(\lambda_n R)\left(Bi + \dfrac{\lambda_n^2 R^2}{Bi}\right)}. \tag{26}$$

Substituting the expression for E_n in equation 26 into the general solution in equation 24 yields the final equation for temperature:

$$\Theta = T - T_\infty = 2Bi\,\Theta_0 \sum_{n=1}^{\infty} \frac{e^{-\alpha \lambda_n^2 t}\, J_0(\lambda_n r)}{(\lambda_n^2 R^2 + Bi^2)\, J_0(\lambda_n R)}. \tag{27}$$

2.2 Solution Technique

Solution of equation 27 for penetrator temperature requires a defined one-dimensional penetrator geometry, necessary boundary and initial conditions, appropriate material properties, and the eigenvalues that satisfy equation 22. The geometry considered is approximately the same as the main body portion of the penetrator used in Guidos and Weinacht (1993), depicted in Figure 2. The radius, R, was 12.5 mm. The convective heat transfer coefficient, h, adiabatic wall temperature temperature, T_∞, and initial temperature, T_0, were 1,700 W/m^2-K, 1285 K, and 295 K, respectively for a penetrator velocity of approximately 1,500 m/s (Guidos and Weinacht 1993). The material properties used for each material are listed in Table 1.

Table 1. Material properties for WHA and DU penetrators (Weast 1975).

	k (W/m-K)	ρ (kg/m^3)	c (J/kg-K)
WHA	178	17,650	134
DU	25	18,600	117

The eigenvalues needed to solve the infinite series (equation 27) were obtained using a graphical technique. This process involved plotting equation 22 with λ as the independent variable and identifying the roots of the equation (i.e., recording the values of λ where equation 22 intersects the λ axis). Figures 3 and 4 are plots of
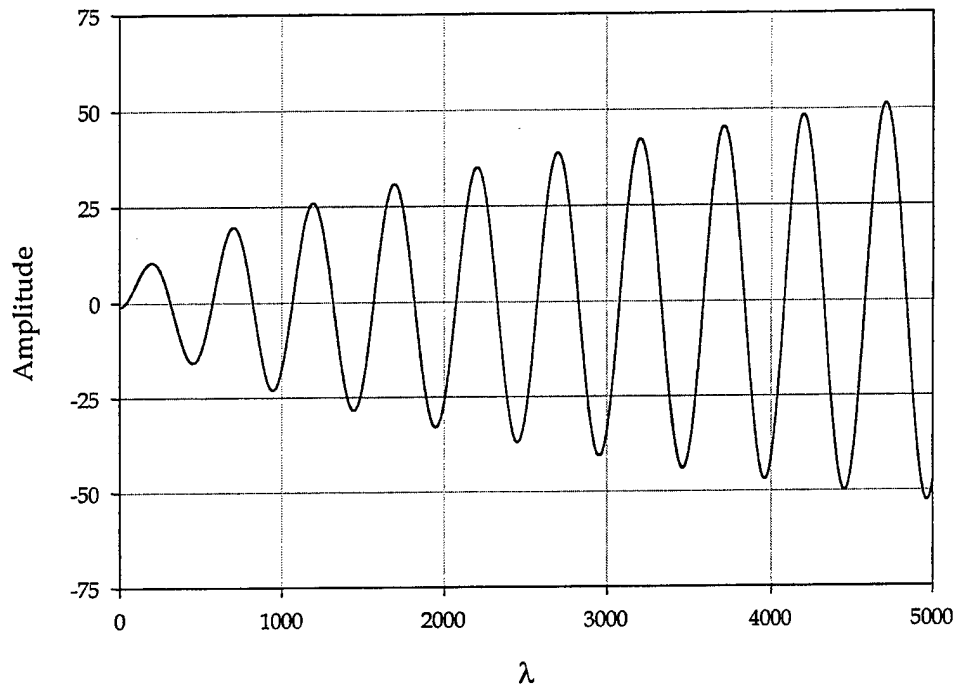
Figure 3. Graphical depiction of characteristic equation for extracting eigenvalues for WHA.
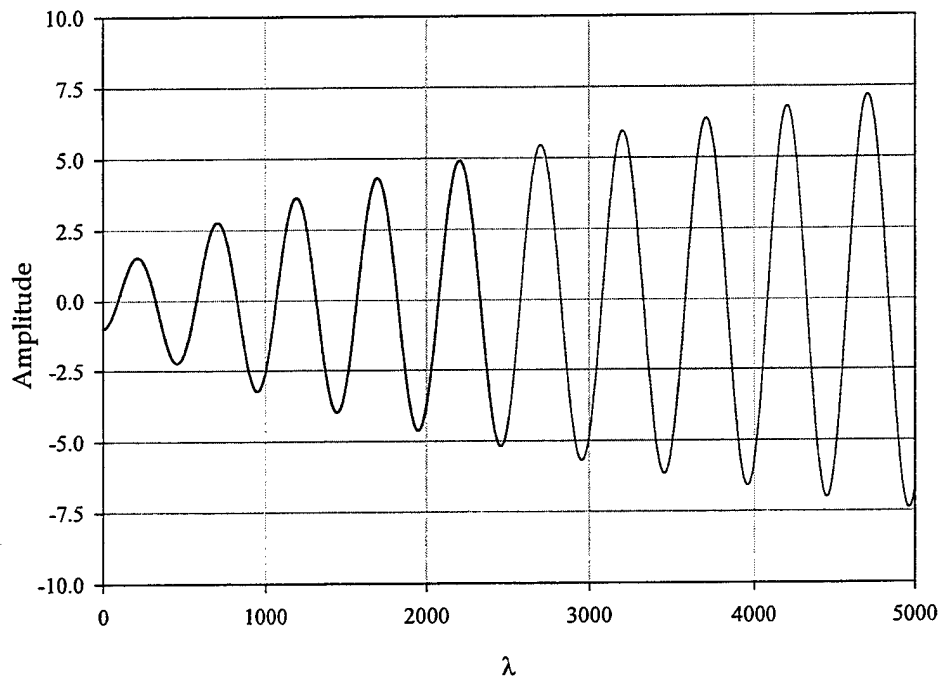

Figure 4. Graphical depiction of characteristic equation for extracting eigenvalues for DU.

equation 22 for WHA and DU, respectively. Since the solution for penetrator temperature involves an infinite series, it was not known *a priori* how many eigenvalues would be needed for solution convergence. As such, the first 20 eigenvalues for each material type were identified and are listed in Table 2. As will be mentioned later, solution convergence occurred rapidly and no additional eigenvalues were needed.

Table 2. First 20 eigenvalues satisfying equation 22 for WHA and DU penetrators.

n	WHA λ_n	DU λ_n
1	38.51	94.21
2	309.02	323.55
3	562.61	570.81
4	814.82	820.52
5	1066.61	1070.98
6	1318.23	1321.77
7	1569.76	1572.73
8	1821.23	1823.79
9	2072.66	2074.92
10	2324.08	2326.08
11	2575.47	2577.28
12	2826.85	2828.51
13	3078.23	3079.75
14	3329.59	3331.00
15	3580.96	3582.26
16	3832.32	3833.54
17	4083.67	4084.82
18	4335.02	4336.10
19	4586.37	4587.39
20	4837.71	4838.68

With the eigenvalues identified, solving equation 27 for penetrator temperature is straightforward. The results presented in the next section were obtained using the first 20 terms of the infinite series expression. Convergence of the solution was observed to occur rapidly. Calculated temperature was found to change less than 0.1 K after the first eight terms of the infinite series for both material types.

3. Results and Discussion

The temperature profile across the penetrator radius was calculated with equation 27 for each material at several flight times. The profiles are plotted in Figures 5 and 6 for WHA and DU, respectively. The temperature increases shown in
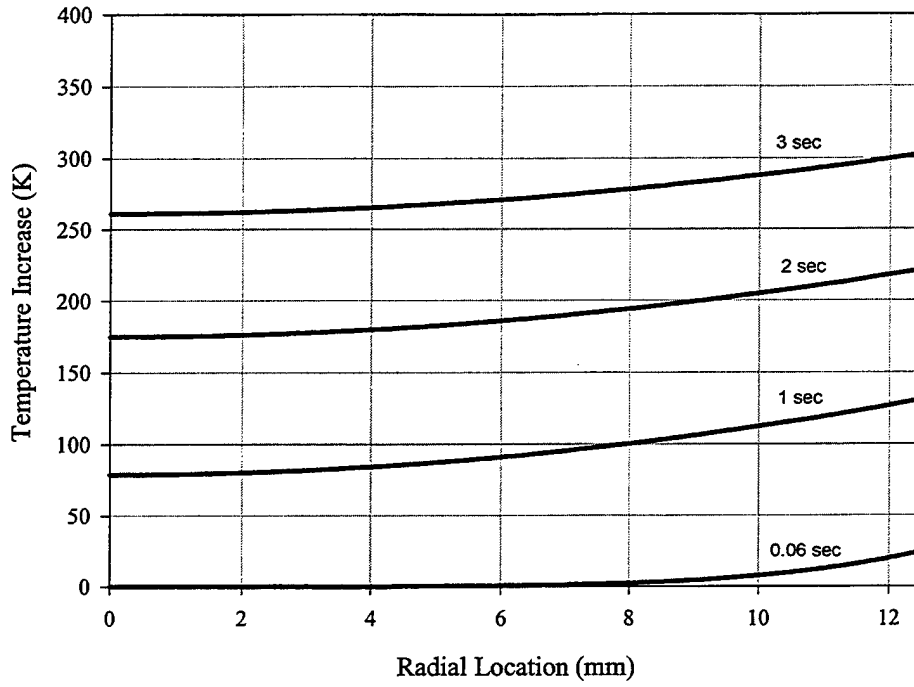
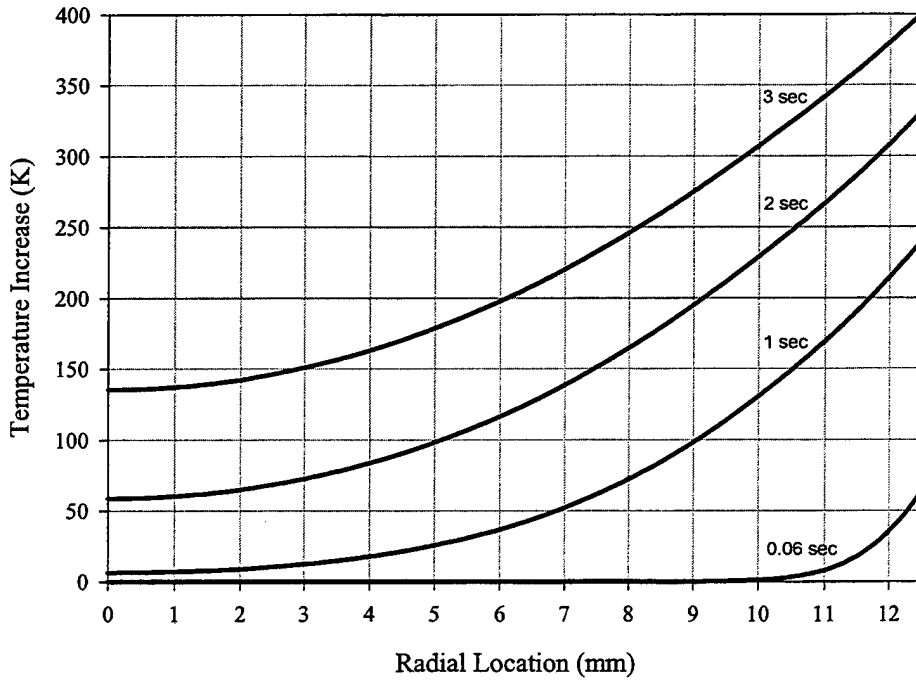Figure 5. Temperature increase inside a WHA penetrator for various flight times.

Figure 6. Temperature increase inside a DU penetrator for various flight times.

both plots are relative to ambient (295 K). The temperature increase on the surface of the WHA penetrator reaches a value of 300 K after 3 s of flight. With a flight speed of 1,500 m/s, this corresponds to an engagement distance of 4.5 km. Penetrator flights as short as 1 s (1.5 km distance) result in surface temperatures of approximately 125 K above ambient. An even shorter flight time of 0.06 s, which corresponds to a typical flight distance for short-range terminal ballistic experiments, results in a temperature increase of about 25 K. The relatively high thermal conductivity of WHA results in very little thermal variation through the radius, thus the entire body of the penetrator is heated to elevated temperatures.

The surface temperature increase for penetrators made of DU were higher than those calculated for WHA. The temperature increase in DU after 3 s was 400 K, compared to 300 K for WHA. The interior region, however, was cooler than the corresponding WHA case. This is due to the low thermal conductivity of DU, which is lower than WHA by a factor of approximately 7. As a result, there exists a significant thermal gradient in the DU penetrator. This was evident even for the shortest flight time considered, 0.06 s, which resulted in a temperature increase of 55 K on the surface and no temperature rise 2.5 mm below the surface.

The ductile-brittle transition temperature of WHA is approximately room temperature under quasi-static loading conditions (Larson and DeLai 1980; Gurwell 1986). The transition temperature will increase for high-rate loadings (Freund 1990), but it is currently unknown how much the increase will be. As such, the calculated temperatures for the WHA penetrator shown in Figure 5 suggest the mode of fracture during a terminal ballistic event may vary, depending on the flight time or distance. Short-range engagements may result in the penetrator undergoing brittle failure, whereas longer flight times may produce ductile failure. Attempts to characterize and model the interaction of the penetrator with a complex armor that applies lateral loading will likely need to account for the difference in fracture behavior of the penetrator material.

The temperature distribution in the DU penetrator offers a different challenge to modeling its terminal ballistic performance. For this material, a significant thermal gradient develops through the radius of the penetrator. Although the mode of fracture will likely remain ductile because of the relatively low transition temperature (Eckelmeyer 1991), a crack originating at the surface of the penetrator will propagate into material that has a decreasingly lower yield stress. Berger et al. (1993) performed crack propagation experiments with steel that had thermal gradients through the thickness, where the crack propagated into higher temperature material. The experiments showed fracture toughness to increase with material temperature, thereby leading to crack arrest when it propagated to material with a high enough temperature. Similar effects will likely be present for DU penetrators at intermediate and long flight times, except in this case the gradient will promote unstable crack growth.

4. Conclusions

A one-dimensional transient heat conduction model was derived to provide the temperature distribution inside a KE penetrator made from either WHA or DU traveling through air at 1,500 m/s. The governing equation was solved using the separation of variables technique, resulting in an infinite series expression for the penetrator radial temperature distribution. A flight time of 3 s was sufficient to raise the temperature of the penetrator surface by 300 and 400 K for WHA and DU, respectively. The surface temperature increase calculated for a much shorter flight time of 0.06 s was 25 K for WHA and 60 K for DU. The high thermal conductivity for WHA resulted in a somewhat uniform radial temperature distribution. The heat absorbed at the penetrator surface was quickly conducted to the interior of the penetrator body. In contrast, the low thermal conductivity of DU suppressed thermal conduction, resulting in a high surface temperature with a significant thermal gradient across the penetrator radius.

The temperatures calculated in this study are significant from the perspective of modeling the terminal ballistic interaction of WHA and DU penetrators with complex armors, particularly when fracture is considered. The proximity to the ductile-brittle transition temperature to the temperatures calculated for the WHA case indicate that fracture mode transition must be considered when developing failure models. Additionally, the thermal gradients calculated for the DU penetrator may have significant implications regarding dynamic crack propagation, which may also need to be accounted for in detailed failure models.

INTENTIONALLY LEFT BLANK.

5. References

Berger, J. R., J. W. Dally, R. deWitt, and R. J. Fields. "A Strain Gage Analysis of Fracture in Wide Plate Tests of Reactor Grade Steel." *Journal of Pressure Vessel Technology*, vol. 115, pp. 398–405, 1993.

Eckelmeyer, K. H. "Uranium and Uranium Alloys." *Metals Handbook, Volume 2: Properties and Selection*, Metals Park, OH: ASM International, 1991.

Freund, L. B. *Dynamic Fracture Mechanics*. Cambridge, England: University of Cambridge Press, 1990.

Greenberg, M. D. *Advanced Engineering Mathematics*. Englewood Cliffs, NJ: Prentice Hall, 1988.

Guidos, B. J., and P. Weinacht. "Parabolized Navier-Stokes Computation of Surface Heat Transfer Characteristics for Supersonic and Hypersonic KE Projectiles." ARL-TR-191, U.S. Army Research Laboratory, Aberdeen Proving Ground, MD, 1993.

Gurwell, W. E. "A Review of Embrittlement Mechanisms in Tungsten Heavy Alloys." Proceedings of the Annual Powder Metallurgy Conference and Exhibition, Boston, MA, 1986.

Larson, F. R., and A. J. DeLai. "Some Considerations for the Ductility of Liquid-Phase Sintered-Tungsten Composites." Proceedings of the 2nd High Density KE Penetrator Materials Conference, Charlottesville, VA, 1980.

Magness, L. S., and C. Lopatin. "Split Hopkinson Bar Compression Screening Tests of High Density Penetrator Materials." Proceedings of the Army Symposium on Solid Mechanics, Plymouth, MA, 1993.

Poulikakos, D. *Conduction Heat Transfer*. Englewood Cliffs, NJ: Prentice Hall, 1994.

Weast, R. C. (editor). *CRC Handbook of Chemistry and Physics*. Cleveland, OH: CRC Press, 1975.

Zurek, A. K., and P. S. Follansbee. "A Comparison of Shear Localization Susceptibility in U-0.75 Wt. Pct. Ti and W-Ni-Fe During High Strain Rate Deformation." *Metallurgical and Materials Transactions A*, vol. 26a, pp. 1483–1490, 1995.

INTENTIONALLY LEFT BLANK.

NO. OF COPIES	ORGANIZATION
2	DEFENSE TECHNICAL INFORMATION CENTER DTIC OCA 8725 JOHN J KINGMAN RD STE 0944 FT BELVOIR VA 22060-6218
1	HQDA DAMO FDT 400 ARMY PENTAGON WASHINGTON DC 20310-0460
1	OSD OUSD(A&T)/ODDR&E(R) DR R J TREW 3800 DEFENSE PENTAGON WASHINGTON DC 20301-3800
1	COMMANDING GENERAL US ARMY MATERIEL CMD AMCRDA TF 5001 EISENHOWER AVE ALEXANDRIA VA 22333-0001
1	INST FOR ADVNCD TCHNLGY THE UNIV OF TEXAS AT AUSTIN 3925 W BRAKER LN STE 400 AUSTIN TX 78759-5316
1	US MILITARY ACADEMY MATH SCI CTR EXCELLENCE MADN MATH THAYER HALL WEST POINT NY 10996-1786
1	DIRECTOR US ARMY RESEARCH LAB AMSRL D DR D SMITH 2800 POWDER MILL RD ADELPHI MD 20783-1197
1	DIRECTOR US ARMY RESEARCH LAB AMSRL CI AI R 2800 POWDER MILL RD ADELPHI MD 20783-1197

NO. OF COPIES	ORGANIZATION
3	DIRECTOR US ARMY RESEARCH LAB AMSRL CI LL 2800 POWDER MILL RD ADELPHI MD 20783-1197
3	DIRECTOR US ARMY RESEARCH LAB AMSRL CI IS T 2800 POWDER MILL RD ADELPHI MD 20783-1197

ABERDEEN PROVING GROUND

NO. OF COPIES	ORGANIZATION
2	DIR USARL AMSRL CI LP (BLDG 305)

NO. OF COPIES	ORGANIZATION
1	COMMANDER US ARMY TRADOC DIR OF TRNG & DOCTRINE DVLPMNT ATZK TS W MEINSHAUSEN FT KNOX KY 40121-5000
3	COMMANDER US ARMY AMCOM AMSAM RD PS WF G SNYDER G JOHNSON D KIELSMEIER REDSTONE ARSENAL AL 35898-5000
1	PROJECT MANAGER KINETIC ENERGY MISSILES PROJECT OFFICE SFAE MSL KE TM A DYKSTRA REDSTONE ARSENAL AL 35898-5000
1	COMMANDER US ARMY ARDEC AMSTA AR TDC J HEDDERICH PICATINNY ARSENAL NJ 07806-5000
3	COMMANDER US ARMY ARDEC AMSTA AR CCH A S MUSALLI M PALATHINGAL R CARR PICATINNY ARSENAL NJ 07806-5000
1	PROJECT MANAGER TANK MAIN ARMAMENT SYS SFAE GCSS TMA K KIMKER PICATINNY ARSENAL NJ 07806-5000

NO. OF COPIES	ORGANIZATION
2	PROJECT MANAGER TANK MAIN ARMAMENT SYS SFAE GCSS TMA SM R DARCY D GUZIEWICZ PICATINNY ARSENAL NJ 07806-5000
3	COMMANDER US ARMY NGIC LANG SCC W GSTATTENBAUER J MORGAN R AIKEN 220 SEVENTH ST NE CHARLOTTESVILLE VA 22902-5396
2	INST FOR ADV TECH UNIV TEXAS AT AUSTIN S BLESS S SATAPATHY 925 W BRAKER LN SUITE 400 PO BOX 202797 AUSTIN TX 78720-2797
2	LOCKHEED MARTIN VOUGHT SYSTEMS R MELIN EM 36 K HAVENS PO BOX 650003 DALLAS TX 75265-0003
1	RAYTHEON ELECTRONIC SYS K CHRISTIANSEN BLDG 805 M/S B3 PO BOX 11337 TUCSON AZ 85734-1337
2	MILTEC CORPORATION J ELDER B BEAUFAIT SUITE 200 6767 OLD MADISON PIKE HUNTSVILLE AL 35806-2100
1	ALLIANT TECHSYSTEMS INC SECURITY MN11 1780 C CANDLAND 600 SECOND ST NE HOPKINS MN 55343

1	ALLIANT TECHSYSTEMS INC A GAUZENS PO BOX 4648 CLEARWATER FL 33758-4648
	GENERAL DEFENSE ORDNANCE & TACTICAL SYSTEMS L WHITMORE 10101 NINTH ST N ST PETERSBURG FL 33716-3800
2	GRC INTERNATIONAL INC T MENNA W ISBELL PO BOX 6770 SANTA BARBARA CA 93160-6770
1	GENERAL DEFENSE ORDNANCE & TACTICAL SYSTEMS T GRAHAM 4565 COMMERCIAL DRIVE NICEVILLE FL 32578

ABERDEEN PROVING GROUND

36	DIR USARL
	AMSRL WM BC
	  P PLOSTINS
	  J NEWILL
	  B GUIDOS
	  P WEINACHT
	AMSRL WM T
	  B BURNS
	AMSRL WM TC
	  T BJERKE (20 CPS)
	  R COATES
	  E KENNEDY
	  L MAGNESS
	  R MUDD
	  S SCHRAML
	  B SORENSEN
	AMSRL WM TD
	  A DIETRICH
	  K FRANK
	  S SCHOENFELD
	  RAPACKI
	  T WEERASOORIYA

INTENTIONALLY LEFT BLANK.

REPORT DOCUMENTATION PAGE

Public reporting burden for this collection of information is estimated to average 1 hour per response, including the time for reviewing instructions, searching existing data sources, gathering and maintaining the data needed, and completing and reviewing the collection of information. Send comments regarding this burden estimate or any other aspect of this collection of information, including suggestions for reducing this burden, to Washington Headquarters Services, Directorate for Information Operations and Reports, 1215 Jefferson Davis Highway, Suite 1204, Arlington, VA 22202-4302, and to the Office of Management and Budget, Paperwork Reduction Project(0704-0188), Washington, DC 20503.

1. AGENCY USE ONLY *(Leave blank)*	2. REPORT DATE September 2001	3. REPORT TYPE AND DATES COVERED Final, October 2000–May 2001	

4. TITLE AND SUBTITLE
On the Aerodynamic Heating of a KE Penetrator—Conductive Material Heating and Thermal Gradients Prior to Transient Impact Loading

5. FUNDING NUMBERS
1L1601102AH42

6. AUTHOR(S)
Todd W. Bjerke

7. PERFORMING ORGANIZATION NAME(S) AND ADDRESS(ES)
U.S. Army Research Laboratory
ATTN: AMSRL-WM-TC
Aberdeen Proving Ground, MD 21005-5066

8. PERFORMING ORGANIZATION REPORT NUMBER
ARL-TR-2574

9. SPONSORING/MONITORING AGENCY NAMES(S) AND ADDRESS(ES)

10. SPONSORING/MONITORING AGENCY REPORT NUMBER

11. SUPPLEMENTARY NOTES

12a. DISTRIBUTION/AVAILABILITY STATEMENT
Approved for public release; distribution is unlimited.

12b. DISTRIBUTION CODE

13. ABSTRACT*(Maximum 200 words)*

The temperature increase in the main body portion of a kinetic energy penetrator flying at sea level with a speed of 1,500 m/s was calculated using an analytical conduction analysis with a convective boundary condition. The penetrator was modeled as a smooth cylinder of uniform diameter and material properties. The results from a previously published computational fluid dynamics simulation were used to provide the convective heat transfer coefficient and the temperature of the gas flowing over the surface of the penetrator. A separation of variables solution was used for the parabolic time-dependent conduction equation. The derived solution along with material properties for tungsten and depleted uranium were used to obtain the temperature increase profile through the radius of the penetrator as a function of flight time. Both materials showed significant heating within 3 s of flight. The tungsten penetrator exhibited nearly uniform heating across the radius, whereas heating of the depleted uranium penetrator was confined to the outermost region of the cylinder due to its low coefficient of thermal conductivity.

14. SUBJECT TERMS
projectile heating, kinetic energy penetrator, aeroballistic heating

15. NUMBER OF PAGES
20

16. PRICE CODE

17. SECURITY CLASSIFICATION OF REPORT UNCLASSIFIED	18. SECURITY CLASSIFICATION OF THIS PAGE UNCLASSIFIED	19. SECURITY CLASSIFICATION OF ABSTRACT UNCLASSIFIED	20. LIMITATION OF ABSTRACT UL

INTENTIONALLY LEFT BLANK.